Research Article

NMR IN BIOMEDICINE

Received: 29 March 2009, Revised: 23 July 2009, Accepted: 27 July 2009, Published online in Wiley InterScience: 30 November 2009

(www.interscience.wiley.com) DOI:10.1002/nbm.1443

Longitudinal MRI and MRSI characterization of the quinolinic acid rat model for excitotoxicity: peculiar apparent diffusion coefficients and recovery of N-acetyl aspartate levels

Noam Shemesh[a†] and Ofer Sadan[b†]Eldad Melamed[b], Daniel Offen[b] and Yoram Cohen[a*]

Quinolinic acid (QA) induced striatal lesion is an important model for excitotoxicity that is also used for efficacy studies. To date, the morphological and spectroscopic indices of this model have not been studied longitudinally by MRI; therefore the objectives of this study were aimed at following the lesion progression and changes in N-acetyl aspartate (NAA) as viewed by MRI and MRSI, respectively, *in-vivo* over a period of 49 days. We found that the affected areas exhibited both high and low apparent diffusion coefficients (ADC) even 49 days post QA injection in three of the six tested animals. MRI-guided histological analysis correlated areas characterized by high ADCs on day 49 with cellular loss, while areas characterized by lower ADCs were correlated with macrophage infiltration (CD68 positive stain). Our MRSI study revealed an initial reduction of NAA levels in the lesioned striatum, which significantly recovered with time, although not to control levels. Total-striatum normalized NAA levels recovered from 0.67 ± 0.15 (of the contralateral row) on day 1 to 0.90 ± 0.12 on day 49. Our findings suggest that NAA should be considered as a marker for neuronal dysfunction, in addition to neuronal viability. Some behavioral indices could be correlated to permanent neuronal damage while others demonstrated a spontaneous recovery parallel to the NAA recovery. Our findings may have implications in efficacy-oriented studies performed on the QA model. Copyright © 2009 John Wiley & Sons, Ltd.

Keywords: Quinolinic acid; Huntington's disease; MRI; MRS; Magnetic Resonance; N-acetyl aspartate recovery; excitotoxicity; diffusion; diffusion MRI; DWI

INTRODUCTION

Excitotoxicity is an important biological process which contributes to neurodegeneration in diseases such as Huntington's disease (HD), Parkinson's disease (PD) and amyotrophic lateral sclerosis (ALS). Quinolinic acid (QA) is an endogenous metabolite of tryptophan and is found in normal subjects as a byproduct along the kynurenine pathway leading to the synthesis of the essential co-factors nicotinic acid and nicotinamide adenine dinucleotide (NAD). Injection of QA to the striatum induces excitotoxicity via N-Methyl-D-Aspartate (NMDA) receptor activation and probably also by endogenous glutamate release (1). These specifically affect the medium spiny striatal neurons and slowly induce striatal degeneration. The QA injection model was considered for many years as a rodent model that mimics the earlier stages of HD (2–4). Since the advent of transgenic models for HD (5,6), the QA-induced striatal lesion became more relevant as a model for excitotoxicity. However, the QA model is still widely used in efficacy studies (4,7–9).

Magnetic resonance imaging (MRI) is the most important imaging modality for following pathology and neurodegeneration non-invasively in the central nervous system (CNS). The high spatial resolution of MRI can faithfully depict the state of pathology through various mechanisms, and biochemical

* *Correspondence to: Y. Cohen, School of Chemistry, The Raymond and Beverly Sackler Faculty of Exact Sciences, Tel Aviv University, Ramat Aviv, Tel Aviv 69978, Israel.*
E-mail: ycohen@post.tau.ac.il

a *N. Shemesh, Y. Cohen*
School of Chemistry, The Raymond and Beverly Sackler Faculty of Exact Sciences, Tel Aviv University, Israel

b *O. Sadan, E. Melamed, D. Offen*
Laboratory of Neurosciences, Felsenstein Medical Research Center, Department of Neurology, Rabin Medical Center, Sackler Faculty of Medicine, Tel Aviv University, Israel

Contract/grant sponsor: Norma and Alan Aufzein Chair for Research in Parkinson's Disease.

† *These authors have contributed equally to this paper.*

Abbreviations used: *3-NP, 3-nitropropionic acid; ADC, apparent diffusion coefficient; CNS, central nervous system; cl, contralateral; DWI, diffusion weighted imaging; EPI, echo planar imaging; FOV, field of view; NAA, N-Acetyl Aspartate; HD, Huntington's disease; MR, magnetic resonance; MRI, magnetic resonance imaging; MRSI, magnetic resonance spectroscopic imaging; PBS, phosphate saline buffer; QA, quinolininc acid.*

NMR IN BIOMEDICINE

information can be obtained through MR spectroscopy (MRS) studies, although with lower spatial resolution. These can elucidate the temporal and spatial evolutions of the toxin-induced neuropathology, which are important determinants of animal model studies (10).

Although the role of N-Acetyl Aspartate (NAA) in the CNS is not clear yet, its levels are considered an important non-invasive marker for neuronal integrity and viability (11). However, several particularly interesting studies in the injection of the mitochondrial toxin 3-Niropropionic acid (3-NP) have shown that in some cases, NAA levels can undergo recovery (12,13), implying that NAA may also be a marker for neuronal dysfunction linked to energy metabolism (11), in addtion to neuronal death.

The 3-NP model has been widely investigated by MR (12,14–18). However, a comprehensive longitudinal MR study has not been performed yet on the QA model, although a few MR studies have shown the evolution of the lesion (19,20) while others have shown NAA levels in a dose response manner in one time-point (21,22). We performed *in-vivo* multiparametric MRI and MRSI that extended over 49 days to assess the spatial and temporal evolution of the QA neuropathology. We tested the relevance of our findings to the behavioral findings of the rats, and finally performed the end-point histology analysis to validate the MRI findings.

MATERIALS AND METHODS

Quinolinic acid induced striatal lesion

Male Wistar rats ($n = 15$, Harlan, Israel) weighing about 280 g were used. All experimental protocols were approved by the University Committee of Animal Use for Research and Education. The rats were placed under 12 h light/12 h dark conditions and grown in individually ventilated cages (IVC) with *ad libitum* access to food and water. Every effort was taken to reduce the number of animals used and to minimize their suffering.

The QA injection protocol and coordinates were previously described (23). Briefly, QA (Sigma-Aldrich, St. Louis, MO, USA) was dissolved in 1M NaOH solution, and then titrated with phosphate buffer to pH 7–7.4. 150 nmol were injected in 1 μL using a stereotactic frame (Stoelting, Wood Dale, IL, USA) under chloral hydrate anesthesia ($n = 6$). The injection was aimed to the left mid-striatum according to the rat brain atlas (24) at the following coordinates (relative to the bregma and dura): Anterior + 0.7 mm, lateral + 2.7 mm, ventral −4.8 mm. The injection rate was 0.5 μl/min, and the inserted needle was withdrawn after 5 min. The QA-injected group ($n = 6$) underwent MRI, MRSI ($n = 5$) and behavioral tests. The control groups ($n = 9$) received 1 μl of PBS to the same location. One control group ($n = 3$) served as a control for the MRSI study and another control group ($n = 6$) served as a control for the behavioral studies.

MRI and MRSI

MR studies were performed on a 7.0 T/30 cm horizontal bore Bruker Biospec (Karlsruhe, Germany) MRI scanner equipped with a gradient system capable of producing gradient pulses of up to 400 mT/m. A body coil was used as the transmit coil, and a 15 mm quadrature coil (Bruker, Karlsruhe, Germany) dedicated for the rat brain was used as the receiving coil.

Anesthesia was induced with ~4% isoflurane (Vetmarket Ltd., Petah Tikva, Israel) and maintained with 1–2% isoflurane in 95% O_2 at a flow rate of 0.3–0.5 l/h. Respiratory rate was monitored throughout the entire MR experiments and was maintained between 40–60 breaths/min. Body temperature was maintained by a feedback system of circulating water at 39°C. MR experiments were performed one day after QA injection (day 1) and on days 8, 25 and 49 post QA injection. The MRI experiments consisted of 2D T_2 weighted images acquired with the following parameters: RARE8 TR/TE = 3500/75 ms, field of view (FOV) of 2.56 cm isotropic, matrix size of 256 × 128 zero filled to 256 × 256 resulting in an in-plane resolution of 100 × 100 $(\mu m)^2$, and the number of scans was four. The DWI-EPI images were collected with the following parameters: TR/TE = 2800/54.5 ms, $\Delta/\delta = 40/4.5$ ms, 2 points with G = 0 mT/m and 173 mT/m in the × direction resulting in b values of 1.5 s/mm^2 and 1500 s/mm^2 respectively. The FOV was 2.56 cm isotropic, the matrix size was 128 × 128 resulting in an in-plane resolution of 200 × 200 $(\mu m)^2$ and the number of scans was four. For both MRI scans, a 1 mm slice thickness was chosen, and ten contiguous coronal slices were collected. ADC maps were calculated from the diffusion weighted images using MatLab 7.3.0. Outer volume suppression was not employed in this study. The MRSI study was performed by a water suppressed 2D MRSI scan with TR/TE = 2000/135 ms, FOV of 2.56 cm isotropic, the matrix size was 8 × 8 zero filled to 16 × 16 and a slice thickness of 4 mm was chosen. The number of scans was 16, and the total scan time was 23 min. The dual purpose of choosing an echo time of 135 ms was the suppression of the majority of the lipid signals by relaxation and refocusing of the J-coupled metabolites such as lactate. VAPOR water suppression scheme was used (25) with a bandwidth of 200 Hz. The slice of interest was shimmed selectively by a volume selective PRESS sequence and resulted in line widths of 12–22 Hz for the water peak.

Due to the longitudinal nature of the study, special care was taken in positioning the slices such that the same slices were sampled along the time-points, and that the rat brain was centered in the same place in every slice. To ensure that the positioning was accurate, an initial T_2 weighted scan was acquired in the beginning of every MRI session. In the first MRI session, the T_2 scan was adjusted such that the first slice always revealed the posterior border of the olfactory bulb. The distance between the midline of the brain, as apparent in the T_2 weighted images, and the edges of the T_2 weighted image were then measured. In subsequent scans, the slices from the T_2 images were carefully adjusted in the anterior-posterior direction such that the slices from the current measurement accurately corresponded to the images from the first MRI session. The distance between the midline and the edges were measured again, and the coordinates were then rectified to correspond exactly to the coordinates from the first session. Only then did the MRI scans take place. The MRSI grid was always placed exactly on the same four slices, and covered the same FOV, ensuring that the voxels were accurately aligned and could be compared longitudinally.

Analysis of MRSI results

One rat (from the QA-injected group) was excluded from the study because it failed to pass the Shapiro-Wilk normality test (*vide infra*). The MRSI results (QA-injected group $n = 5$ after exclusion of one rat, control group $n = 3$) were zero filled to 8 k, multiplied by a line broadening factor of 10, then phase-corrected. The spectra from all of the voxels of interest were imported to Mestre-C software (26). The NAA peak was then fitted

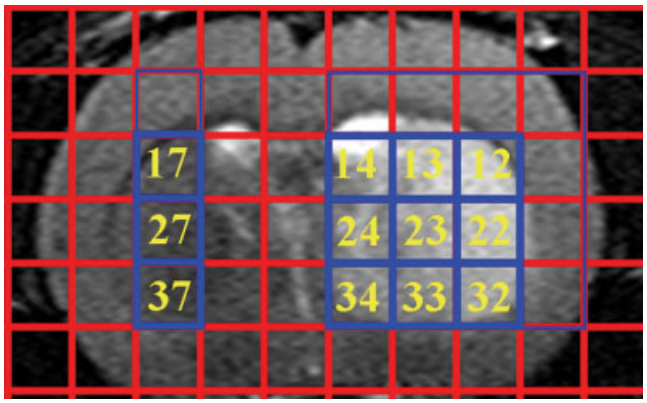

Figure 1. The MRSI grid, used for NAA analysis in this study, overlaid on the T_2 weighted image taken on day 1 post QA injection. Normalized NAA levels were calculated by dividing the voxel of interest with one voxel from the same contralateral row. NAA levels of voxels, voxels 12–14 were normalized to voxel 17, voxels 22–24 were normalized to voxel 27 and voxels 32–34 were normalized to voxel 37.

to a Lorentzian function and the area under the peak was generated from the fitted function. The NAA levels in each voxel in every row were normalized to one representative contralateral voxel in the same row. Only voxels from the striatum were analyzed. The NAA levels of voxels 12–14 (Fig. 1) were all normalized to voxel 17, voxels 22–24 were normalized to voxel 27 and voxels 32–34 were normalized to voxel 37. Voxels 17, 27 and 37 were named 'contralateral' (cl) for the analysis of NAA levels. The normalized NAA levels were defined as the ratio of NAA_{ipsi}/NAA_{cl}. We did not normalize NAA levels to total-Creatine or total-Choline levels since we could not assume that these metabolites remain constant for 49 days post QA-injection, in light of the recent reports showing changes in these metabolites already 5 days post QA-injection (21).

To study the normalized NAA levels from the striatum as a whole, we first employed a pseudo 'single voxel' approach, by combining normalized NAA levels from all of the voxels in the striatum. Normalized NAA levels from voxels 12–14, 22–24, 32–34 (Fig. 1) were added and their mean $\pm$ stdv was computed for each animal for every time point. This ensemble of striatum voxels was termed Total-striatum normalized NAA levels.

We then sought to study how NAA levels from voxels with different degrees of initial impairment develop with time. Therefore, the normalized NAA levels from the striatum were then divided into three groups: Voxels in which NAA_{ipsi}/NAA_{cl} levels had been at least 0.8 on day 1 were assigned as 'mild' impairment voxels. Voxels in which NAA_{ipsi}/NAA_{cl} levels had been between 0.8 and 0.6 on day 1 were assigned as moderate impairment voxels. Voxels in which NAA_{ipsi}/NAA_{cl} levels had been between 0.6 and 0.3 on day 1 post QA injection were assigned as severe impairment voxels. Each class of voxels passed the Shapiro-Wilk normality test (OriginPro 7.5) and was analyzed by its impairment classification at the subsequent time-points. The same voxels were always analyzed along the time course of the experiments.

Behavioral studies

Apomorphine induced rotations

Rats ($n = 12$) were weighed weekly. From the 7th day post QA injection, and in a 2 week interval along the experiment, rats were treated with apomorphine (Sigma-Aldrich) 1 mg/Kg subcutane (SC) and net ipsilateral rotations were automatically monitored for 45 min by a rotameter (San Diego Instruments, San Diego, CA, USA).

Open field

In order to test the QA-induced behavioral changes, rats ($n = 12$) were placed in a black 45 cm^2 square open-field arena, with a 30-cm high plastic wall. The surroundings were visually uniform and illuminated by a dimmed light projected on the walls of the examination room. The arena was virtually divided into three zones by two squares: the perimeters near the walls, the center and the area between them. The arena was carefully cleaned with ethanol before every test. Rats were placed in the arena for 60 min on the 5th and the 12th week post treatment. All tests were video-recorded and analyzed by Ethovision 3.0 software (Noldus, The Netherlands). The following parameters were measured: total distance moved in cm, mean velocity (cm/s), percent of the time the animal was mobile (defined as a change of more than 10% of the pixels marking the animal body between two frames, taken at five frames per sec), percent of the time the animal presented a strong movement (defined as 30% in the same manner as mobile), time in the perimeter zone and in the center. For anxiety-related behavior the percent of the time the animal spent in the center and the perimeters was measured as previously described (27).

Immunohistochemistry

On day 70, two of the three rats that exhibited both low and high ADCs were anesthetized with chloral hydrate for MRI guided histology. Animals were intracardially perfused with ice cold PBS for 5 min, followed by 15 min of 4% paraformaldehyde. Brains were removed and immersed in 4% paraformaldehyde for 48 h in 4°C and cryoprotected in 30% sucrose for another 48 h. After immersion, the tissues were frozen in −70°C until they were cryosectioned to 10 μm coronal sections. Sections were incubated in a blocking and permeabilization solution (5% normal goat serum, 1% bovine serum albumin and 0.5% Triton X100 in PBS) and incubated with a primary antibody overnight at 4°C (mouse anti CD68 (ED1, a macrophage marker) 1:500, Serotec, Oxford, UK). After washing with PBS, sections were incubated with a biotinilated secondary antibody (Gout anti-mouse, Invitrogen, Carlsbad, CA, USA, ready to use) for 1 h followed by DAB staining using Vector ABC kit (Vector, Peterborough, UK).

Statistical analysis

MRSI data

Longitudinal results for NAA levels underwent unpaired *t*-tests (OriginPro 7.5). Significant P values are indicated where appropriate.

Behavioral test and histology

Student's *t*-test was used to compare the two groups. Statistical calculations were performed using SPSS v. 13. All results are expressed as means $\pm$ standard error, unless stated otherwise. In order to determine the correlation between open field tested parameters, we employed a linear regression, and conducted a *t*-test on the beta coefficient for determining statistical significance of the correlation.

NMR IN BIOMEDICINE

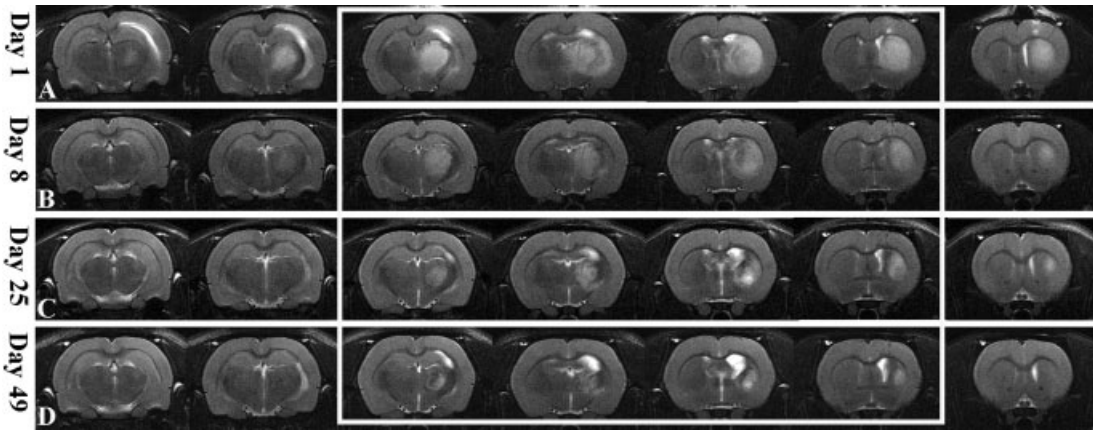

Figure 2. Coronal T_2 weighted images of one representative rat. (a) Day 1, (b) day 8 (c) day 25 and (d) day 49 post QA injection. Only seven contiguous slices out of the ten acquired are shown. Note that the lesion is confined to the striatum. The initial edema subsides by day 8 to leave a marked striatal lesion. The slices marked by a white box comprise the MRSI slice.

RESULTS

Magnetic resonance imaging

Figure 2 shows the longitudinal coronal T_2 weighted images from one representative rat post QA injection. In these images, the affected areas, found mostly in the striatum, appeared hyperintense. One day post QA injection, a mild enlargement of the ipsilateral ventricle could be seen (Fig. 2a). The abnormalities as seen in the T_2 weighted images were clearly observable over six to seven slices in all of the six animals injected with QA. The ventricles asymmetry subsided with time and by day 8 no abnormalities in the posterior parts of the ventricle could be found (Fig. 2b). The edema substantially decreased and the hyperintensity in T_2 weighted images was somewhat diminished (Fig. 2b). The hyperintensity in the striatum slowly recedes with time, and on day 25 the lesion appears smaller and less intense (Fig. 2c). Forty-nine days after QA injection, only four slices revealed some hyperintensity in the striatum (Fig. 2d). It should be noted that the ventricles appear somewhat enlarged along the entire time course of the experiment.

The apparent diffusion coefficients (ADC) maps (Fig. 3) revealed a complex behavior. One day post QA injection the lesion was less apparent in the ADC maps as compared to the T_2 weighted images, and could be seen in only three to four slices as areas of low ADCs, in the range of $0.2–0.6 \times 10^{-3}$ mm^2/sec (Fig. 3a). On day 8, the lesion was still distinguishable (Fig. 3b), and after 25 and 49 days, two types of diffusion abnormalities were observed – a low ADC area, with ADC values in the range of $0.2–0.6 \times 10^{-3}$ mm^2/sec (white arrow) and a high ADC area, with ADC values in the range of $1.5–2.0 \times 10^{-3}$ mm^2/sec (black arrow), (Figs. 3c and 3d respectively). A rim of intermediate ADC value, circa 1.2×10^{-3} mm^2/sec, could be seen around the region with high ADCs, indicating ongoing processes around the necrotic region (black arrowhead). This duality was noted in three of the six rats measured, while in the two other specimens, only areas with high ADCs were detected. One rat showed no abnormalities (in both T_2 and diffusion weighted images) from day 25.

Magnetic resonance spectroscopy

The raw data of the MRSI scan from one representative QA-injected rat on day 1 post QA injection and one representative control are shown in Figures 4a and 4b, respectively. It should be noted that due to partial volume effects arising from the most anterior part of the brain included in the slice, some non-brain tissue lipid signals can be seen in the external cortical voxels. Therefore, only voxels 12–14, 22–24 and 32–34 were analyzed. These voxels were referenced to voxels 17, 27 and 37 respectively as explained in the materials and methods section. The baseline in these voxels remained mostly lipid-free. The NAA, creatine, choline and glutamate/glutamine resonances were easily resolved. Additionally, an inverted peak (due to the 135 ms echo time), which was assigned to lactate was detected on day 1 post QA-injection for all animals. From day 8, no lactate signals could be detected.

We examined the total-striatum normalized NAA levels (see materials and methods section and Fig. 1) by employing a pseudo-single voxel approach, i.e. we combined the normalized NAA levels from all of the voxels in the striatum. Figure 5a depicts the total-striatum normalized NAA levels between days 1 and 49 post QA injection. On day 1, total-striatum normalized NAA levels were reduced to 0.67 ± 0.15 of the contralateral. On day 8, the total-striatum normalized NAA levels did not show a statistically significant difference compared to day 1 and remained at 0.68 ± 0.17. On day 25, a statistically significant partial recovery of total-striatum normalized NAA levels to 0.81 ± 0.12 was observed. Forty-nine days after QA injection, total-striatum normalized NAA levels further increased to 0.90 ± 0.12, significantly different from total-striatum normalized NAA levels on days 25, 8 and 1 post QA injection. It should be noted that the total-striatum normalized NAA levels of the QA-injected group on day 49 were still lower than the total-striatum normalized NAA levels of the control (injected with PBS) group with a statistically significant difference ($p < 0.05$). For the control group, total-striatum normalized NAA levels were found to be 1.00 ± 0.06 ($n = 3$).

We then examined the NAA levels according to the impairment classifications we defined (Fig. 5b). The fractions of voxels in which normalized NAA levels were assigned as mild, moderate and severe impairment (Fig. 5b) were found to be 0.13, 0.57 and 0.30 respectively. Interestingly, choosing other cutoff levels resulted in failure of the normality test.

Normalized NAA levels from mild impairment voxels (Fig. 5c) were lowered to 0.90 ± 0.10 on day 1 post QA injection. These voxels did not exhibit any significant changes compared to the earlier time-points, until day 49, on which normalized NAA levels

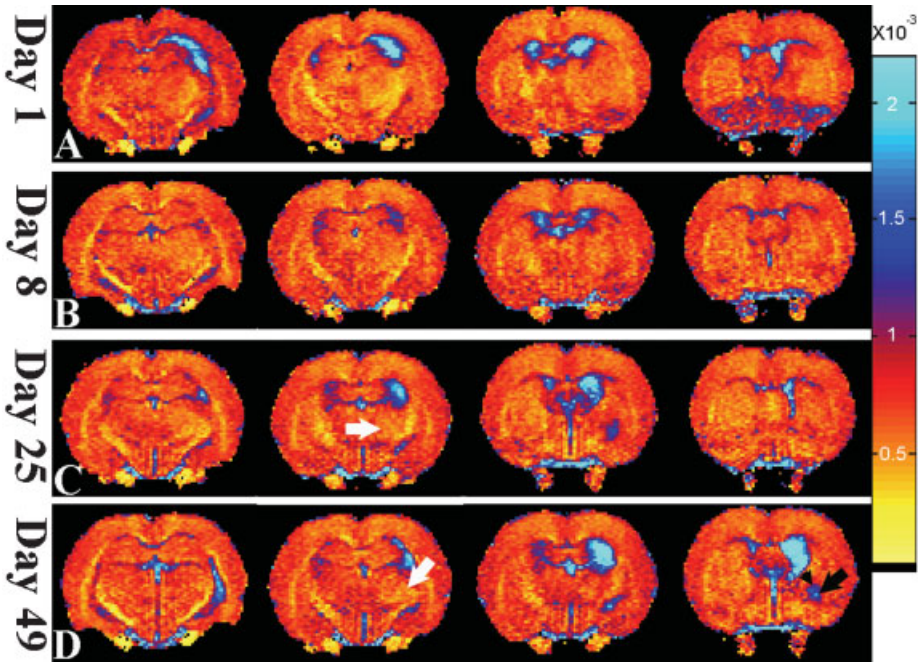

Figure 3. Coronal ADC maps of one representative rat. (a) Day 1, (b) day 8 (c) day 25 and (d) day 49 post QA injection. Only four contiguous slices out of the ten acquired are shown. Note that the ADC map reveals areas characterized by low ADCs on day 1. On days 25 and 49, two distinct abnormalities were found: a region that exhibited high ADC values (black arrow, necrotic region) and low ADC values (white arrow). This area corresponded to a dense CD68 positive stain in the histological study. The rim of the high ADC region exhibits intermediate ADC values (black arrowhead, positive stain for CD68), showing that the necrotic region is surrounded by ongoing inflammatory processes. The units for the ADC maps are mm^2/sec

recovered to 1.03 ± 0.07 of the contralateral row. This recovery was statistically significant only when compared to day 1 and 8, but not when compared to day 25. The normalized NAA levels in moderately impaired voxels (Fig. 5d) initially dropped to 0.71 ± 0.05. On day 8, these voxels did not show any statistically significant difference as compared to day 1, and normalized NAA levels in these voxels were found to be 0.67 ± 0.15. After 25 days, normalized NAA levels in moderately impaired voxels recovered to 0.80 ± 0.12, with a statistically significant difference when compared to days 1 and 8. Forty-nine days post QA injection, normalized NAA levels from these voxels exhibited a statistically significant difference when compared to days 1 and 8 but not when compared to day 25 and were found to be 0.85 ± 0.11. Normalized NAA levels in severely impaired voxels (Fig. 5e) initially dropped to 0.46 ± 0.09 on day 1. On day 8, normalized NAA levels were higher, with a statistically significant difference from day 1 and were found to be 0.67 ± 0.18. Twenty-five days post QA injection, the normalized NAA levels in these voxels further elevated to 0.81 ± 0.12 with a statistically significant difference from the normalized NAA levels that had been observed on day 1 but not on day 8. On day 49 post QA injection, normalized NAA levels of the severely impaired voxels showed a

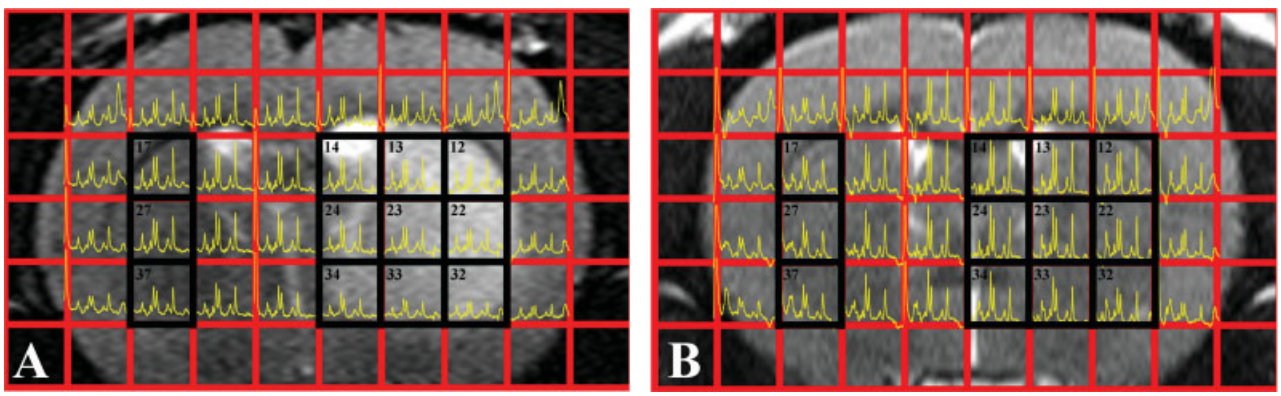

Figure 4. MRSI dataset. (a) Spectra of a representative QA-injected rat 1 day post QA injection and (b) spectra of a control rat. The spectra are overlaid on a T_2 weighted image. On day 1, lactate signals can be observed in the ipsilataeral side. Note that NAA, Creatine and Choline peaks could be easily resolved and the baseline is relatively lipid free due to the 135 ms echo time used in the MRSI sequence. It should be noted that the slice thickness of the T_2 weighted image is only 1 mm, while the slice thickness of the MRSI data is 4 mm. Therefore, the lipid signals in the more external voxels result from contribution of the more anterior part of the brain.

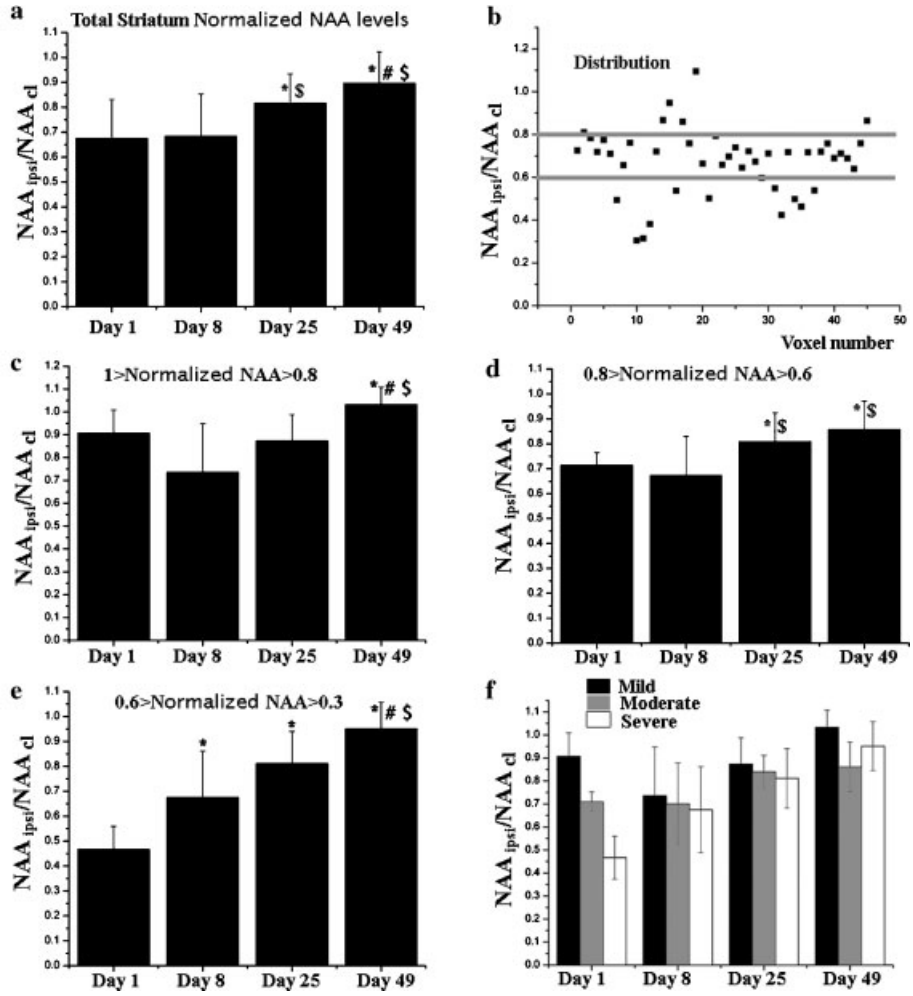

Figure 5. Longitudinal MRSI study of NAA levels. (a) Time course of total-striatum normalized NAA levels. $^{*}p < 0.0001$ *vs* day 1, $^{\$}p < 0.0001$ *vs* day 8 and $^{\#}p < 0.001$ *vs* day 25 (b) Distribution of striatum voxels. The cutoff values for classification of voxels were chosen from this distribution. (c) Time course of mild impairment voxels. $^{*}p < 0.03$ *vs* day 1, $^{\$}p < 0.005$ *vs* day 8 and $^{\#}p < 0.01$ *vs* day 25 (d) Time course of moderate impairment voxels. $^{*}p < 0.0002$ *vs* day 1, $^{\$}p < 0.0001$ *vs* day 8 (e) Time course of severe impairment voxels. $^{*}p < 0.0005$ *vs* day 1, $^{\$}p < 0.0001$ *vs* day 8 and $^{\#}p < 0.0007$ *vs* day 25 (f) Combined time course of all classes of voxels. Note that the total-striatum normalized NAA levels of the QA-injection group on day 49 (a) is significantly lower as compared to the control (PBS-injected) group, $p < 0.05$.

statistically significant difference from all previous time-points and were found to be 0.95 ± 0.10, higher from all previous time -points. The time course of the three classes of voxels can be seen in Figure 5f. Interestingly, the three classes of voxels improved at different rates, with the most severely impaired voxels improving at the fastest rate.

In this study, we chose to normalize NAA levels to a representative voxel from the contralateral row, since we could not assume, *a priori*, no change in other metabolites in the ipsilateral hemisphere. To ensure that the NAA_{ipsi}/NAA_{cl} ratios were not biased by RF inhomogeneity or detection errors, a control group that was injected with PBS was measured using the same acquisition protocol and evaluated by the same scheme. Total-striatum normalized NAA levels from this control group (injected with PBS) were found to be 1.00 ± 0.06 ($n = 3$), indicating that normalization of NAA levels to the contralateral row is indeed accurate in our experimental design. Moreover, in the control group, no statistically significant differences could be found when comparing normalized NAA levels between rows or between columns (data not shown), indicating that RF imperfections or magnetic field inhomogeneity do not alter the results and indeed give normalized NAA levels of 1.00 ± 0.06.

Behavioral studies

Treated rats failed to gain weight for 14 days after treatment with QA. From day 21 on, the treated and control groups gained weight in a parallel fashion, and there was a statistically significant difference between them (Fig. 6a).

Apomorphine induced rotations were elevated compared to control group in a statistically significant manner from the 7th day and throughout all the time-points tested. The QA-treated group showed an increase in the rotational behavior till the 35th day, and from that point on, went into a plateau (Fig. 6b).

In the open field test several QA-induced phenomena were observed. First, the lesioned animals exhibited a hyperactive conduct manifested in a statistically significant longer distance moved in the arena, which correlated well with other parameters such as the percent of the time in which the animals moved (defined as at least 10% movement per frame), strong movement

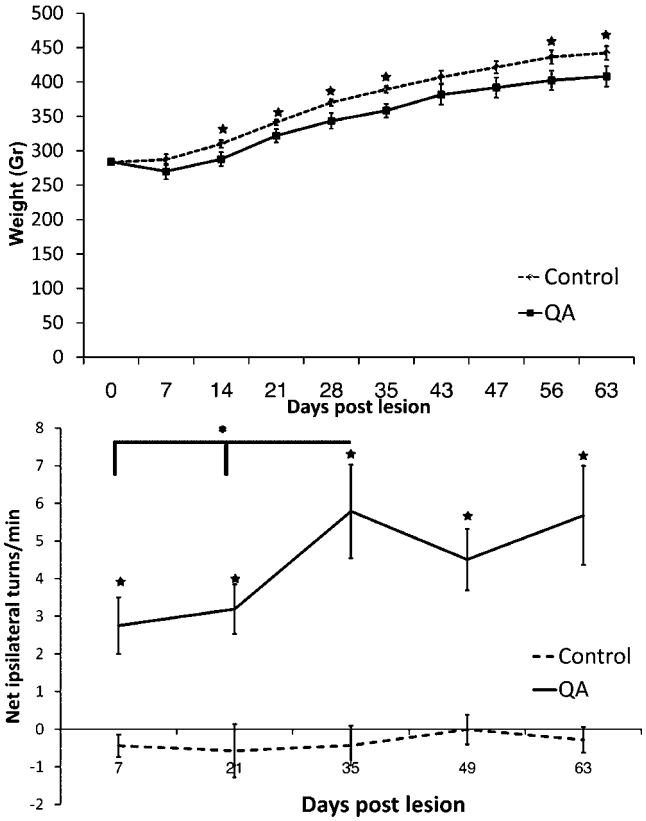

Figure 6. Behavioral tests. (a) Body weight of the animals along the experiment (★- $p < 0.05$ compared to the control group). (b) Apomorphine induced rotation (★- $p < 0.005$ compared to the control group, ✱- $p < 0.05$ compared to earlier time-points in a paired *t*-test).

(defined as 30% and above movement), mean velocity and others (Table 1). A second change was the anxiolitic behavior manifested in a statistically significant higher presence in the middle of the arena and a reciprocal lesser presence in the periphery of the arena in the QA-treated group compared with the control group.

The third remark pertains to the second test conducted 47 days after the first open field test. We found that the control group behaved in a similar manner in both tests ($p = 0.28$ in a paired *t*-test when comparing the total distance moved). However, the QA-treated group revealed a recovery in terms of reduction of the distance moved and other movement-related parameters, as well as anxiety-related parameters. In fact, when we compared the QA injected group to the control group in the later time-point we found no statistically significant differences in all of the parameters tested. When compared to itself along the time course of the experiment, the treated group showed a reduction of the hyperactive behavior ($p = 0.001$), meaning that the spontaneous activity of the QA-lesioned rats was reduced to the control level at 12 weeks post QA injection.

Histology

From a macroscopic view, the histological appearance of the lesioned animals (Figs. 7a, 7f) closely resembled the ADC maps (Figs. 7b, 7g). The most prominent feature that could be seen is the a-symmetric ventricle enlargement in the ipsilesional side. Most importantly, when the sections were stained for the presence of macrophages, there was a clear correlation between the CD68 positive stain (Fig. 7d) and the regions characterized by low ADCs from the ADC maps of day 49 post QA injection (Fig. 7b, right box). Figure 7k shows a single macrophage as viewed by the CD68 positive stain. The high ADC areas on day 49 (Fig. 7g, right box) were found to be a pseudocystic structure, in which a disappearance of a large fraction of cells was noted (Fig. 7i). The T_2 weighted images could not clearly distinguish between the different pathological processes as viewed by histology, although some hypointensity was observed on the T_2 weighted images in the region of reduced ADCs (Figs. 7c, 7h). Staining the contralateral areas for CD68 (Figs. 7e, 7j) did not reveal any significant macrophage infiltration, and the corresponding ADC maps for the contralateral areas reveal normal ADCs (Figs. 7b, 7g, left boxes).

DISCUSSION

Animal models for neurodegenerative diseases and processes are important tools for revealing the underlying mechanisms and for the search of novel treatments. Therefore, a longitudinal characterization of these models is imperative for understanding the progression of the neuropathologies involved.

The QA-induced striatal lesion, which was previously studied as a model for HD, is now considered an important animal model for excitotoxicity. One advantage of this model is its unilaterality which allows an intrinsic control in the contralateral hemisphere, a property which we have utilized in this study. Indeed, several

Table 1. Open field test 5 weeks and 12 weeks post treatment. (★- $p < 0.05$ compared to control, C-correlated to distance with $R^2 > 0.76$, p for beta < 0.05).

	5 weeks		12 weeks	
Parameter	Control	QA	Control	QA
Distance moved (cm)	6695 ± 945	9820 ± 620(★-)	7510 ± 695	6265 ± 420
Mean velocity (cm/s)	1.85 ± 0.26 (C)	2.72 ± 0.17 (★-,C)	2.08 ± 0.19 (C)	1.74 ± 0.11 (C)
Time mobile (%)	19.2 ± 2.5 (C)	28.0 ± 1.7 (★-,C)	25.5 ± 2.1	22.6 ± 5.3
Time strong mobility (%)	2.1 ± 0.5 (C)	4.1 ± 0.7 (★-,C)	5.0 ± 0.9	3.7 ± 1.2
Time in the perimeter (%)	95.3 ± 1.5	82.9 ± 3.9 (★-)	86.9 ± 5.7	88.2 ± 6.4
Time in the center (%)	0.29 ± 0.12	0.78 ± 0.15 (★-)	0.51 ± 0.21	0.95 ± 0.81

NMR IN BIOMEDICINE

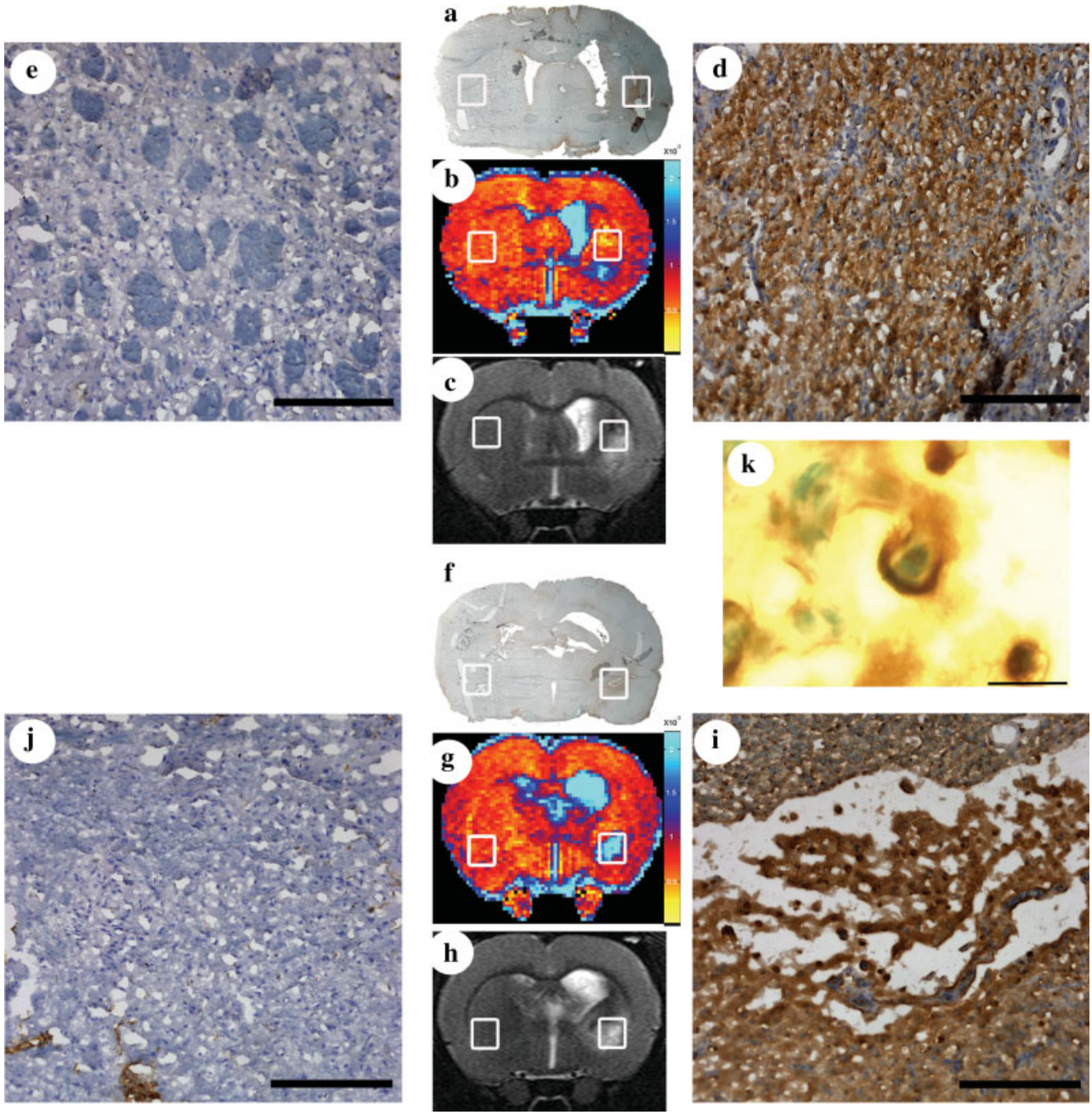

Figure 7. Histological study. (a, f) Histological slices (macro view). (b, g) Corresponding ADC maps (day 49). (c, h) Corresponding T_2 weighted images (day 49). (d, i) CD68 stain (x 100, scale bar = 200 μm) from the regions of interest in the ipsilesional hemisphere. (e, j) CD68 stain from the contralateral hemisphere. (k) A magnified image of a single cell stained for CD68 within the lesion (x 1000, scale bar = 20 μm). Areas characterized by low ADC values (right box in b) exhibited a dense positive stain for CD68 (d) indicating the presence of macrophages and ongoing inflammatory processes. Areas characterized by high ADC values (right box in g) showed a pseudocystic arrangement in the corresponding histological slice (i). The ADC maps reveal the dual status of the lesion much more clearly than the T_2 weighted images. The parallel areas from the contralateral hemisphere exhibit no positive stain for CD68 (e, j).

efficacy studies have employed this animal model, especially in therapeutic-oriented studies in recent years (28–33).

Since MRI enables non-invasive longitudinal studies and access to biochemical and anatomical information, it is the ideal modality to characterize the temporal and spatial evolutions of neuropathologies *in-vivo*. For example, the characterization of ischemic stroke model in MRI has led to better understanding of several underlying biochemical and pathological processes (34–36). In this study, we have longitudinally characterized the QA model from (1) a morphological point of view with the T_2 and diffusion weighted images and (2) a metabolic point of view by focusing on NAA levels.

From the morphological point of view, the QA model progresses through several stages with time. An inflammatory response is induced in the CNS 1 day after QA injection (37,38), depicted as regions of hyperintensity in T_2 weighted images and low ADC values in DWI. The ADC maps on day 8 revealed that low ADCs remained in the striatum, while T_2 weighted images

showed that the edema subsided. The temporal evolution of the lesion as viewed by DWI revealed regions characterized by both low and high ADCs on days 25 and 49. To the best of our knowledge, this is the first study to show such a dual phenomenon at late time-points of pathology. The simultaneous finding of areas characterized by low ADCs in the striatum, as well as intermediate ADC regions in the rim of the necrotic part on day 49 may imply parallel mechanisms in action: low ADCs are considered to arise, *inter alia*, from the shift of water from extracellular to intracellular space during cell swelling, while high ADCs represent freely diffusing water molecules consistent with necrotic regions that had undergone membrane breakdown and removal (39–41). Even though the histological analysis was performed 21 days after the last MR scan, it correlated very well with the DWI results. Areas characterized by high ADCs had pseudocystic characteristics and had undergone cell death and clearance. Interestingly, the regions characterized by low ADCs demonstrated a dense macrophages-positive stain. This implies that the initial inflammatory processes previously described in this model continued for at least 70 days post QA injection, although probably on a smaller scale than in the acute phase, immediately after QA injection.

There are several options for the persistence of low ADCs in the lesion for such a long time. The low ADCs areas shown in this study may possibly arise from cytotoxic edema which propagates due to the ongoing neuropathological processes. Alternatively, the persistence of low ADCs may be due to a change in the tissue density caused by macrophage infiltration, as shown in the histological study. It is noteworthy that only three of the six rats measured revealed areas characterized by both high and low ADCs in the QA-treated group. This indeed reflects the heterogeneity in such toxin-induced studies, and should be taken into account when efficacy studies are performed.

From the metabolic point of view, we focused on N-Acetyl Aspartate levels in the impaired striatum as estimated from the integral of the NAA peak detected by MRSI. It should be noted that quantification of metabolites as detected by MRSI is not straightforward, and is susceptible to relaxation effects, RF inhomogenieties, and normalization strategies.

NAA, which is almost exclusively localized in neurons, was initially considered as a marker for neuronal viability and it had been thought that its depletion arises from death, breakdown and clearance of neuronal tissue (42,43). However, recent studies have shown that in some cases NAA depletion may be reversible, either by therapeutic interventions (44) or spontaneously (12,13,45), suggesting that NAA levels may be also pertinent to neuronal function/dysfunction resulting from shifts in energetic demand (11). This question is crucial since NAA is used as a neurodiagnostic marker for cellular viability (11).

In our study, the early reduction and significant recovery of total-striatum normalized NAA levels, demonstrates that a major population of the neurons in this region was reversibly impaired. Normalized NAA levels in the striatum failed to completely recover to control levels even after 49 days indicating that indeed a relatively small population of irreversibly damaged neurons had probably undergone cell death. We could not correlate the NAA levels to regions that were characterized by high or low ADCs because of partial volume effects. However, it seems probable that at the later time-points of this study, the neuronal loss manifests itself in the high ADC region.

Interestingly, we found a differential rate of improvement for the three classes of voxels: all classes of voxels demonstrated improvement compared to day 1 post QA injection, but surprisingly, the most impaired voxels improved more rapidly. On day 1, the most impaired regions probably suffer severe metabolic stress. This stress may begin to alleviate within a few days, and the areas in which NAA synthesis was most severely shut down may begin to recover, resulting in recovery of NAA levels. Increased neurogenesis (46) is unlikely to induce such a significant recovery of NAA.

We could not completely rule out the possibility the recovery observed was due to iron release on day 1 that caused a T_2 decrease which in turn resulted in detection of lower NAA levels in the early time-points. Upon clearance of iron due to macrophage uptake and departure, the signal can recover over time. However, due to the large changes in NAA levels and the fact that no change was observed in the line shape, it seems unlikely that the above mechanism was of significant importance in the present study. Additionally, in areas which were characterized by high ADCs, the histological analysis revealed a pseudo-cystic arrangement and cell clearance, which would only account for a decrease in NAA levels; however, in this study, an opposite trend was observed.

One can compare the rate of recovery of NAA in severely impaired voxels to that shown in the HPLC study of the systemic 3-NP model (a mitochondrial toxin), which has demonstrated reduction in striatum NAA levels to ~20% of control by day 3 (i.e. severe impairment), and rapid recovery by day 9 (13). In our study, the NAA levels in moderately impaired voxels are somewhat comparable to the sub-acute 3-NP animal model, in which the NAA levels were reduced to roughly 85% and then returned to normal levels after 28 days (18). These studies used single-voxel methods. The heterogeneity in NAA levels that was revealed by our MRSI study may encompass a broader view regarding the nature of recovery of NAA. Our findings imply that indeed NAA should be considered as a marker for neuronal dysfunction, and may be considered a marker of neuronal death only after a prolonged period of time in which the recovery of NAA levels does not persist. Therefore, efficacy studies should take the significant spontaneous recovery of NAA levels in this model into account.

Comparing the NAA recovery to the behavioral studies reveals that NAA recovery precedes the behavioral changes. The behavioral tests included a pharmacologically-induced apomorphine rotational challenge and a spontaneous behavior open field test. The apomorphine-induced rotations demonstrated a consistent impairment throughout the time course of the experiment, without any signs of recovery. This can be attributed to the sensitivity of pharmacologically-induced tests; even a minor impairment to the striatum would give rise to significant rotational behavior. Therefore the partial NAA recovery is not reflected by these tests since indeed the NAA levels did not reach control levels. By contrast, the open field tests, which were performed on 5 and 12 weeks post QA injection, demonstrated the well documented hyperactive and anxiolytic conduct (47–49), followed by an improvement in both of these manifestations in the later test. Most previous studies followed the hyperactive conduct, only up to 4 weeks post QA injections. To the best of our knowledge, this is the first report to show a spontaneous recovery after 12 weeks in the QA model which is associated with the NAA recovery shown in this study. It should be noted that the open field test cannot be conducted in short time intervals due to habituation effects; therefore the time lag documented between the NAA recovery and the behavioral recovery may well be a

manifestation of the experimental design of the present study. The control group demonstrated a consistent behavior in both time-points; therefore it seems that the spontaneous improvement of the QA group was not a result of habituation.

It is important to note that we could note demonstrate a clear spatial correlation between the T_2 findings, the ADC findings, and the MRSI data. T_2 and ADC are two distinct physical parameters. There is no reason to expect an *a-priori* correlation between T_2 and diffusion findings due to their inherently different mechanisms of contrast. The spectroscopic findings were hard to correlate with the morphological changes, since the resolution of our DWI and T_2 data was much higher than our MRSI resolution. Indeed the metabolite MRSI data suffers from partial volume effects; therefore, a comparison with the ADC or T_2 weighted MR images is not straightforward, especially if the MRI abnormalities occupy small areas. In the present study, indeed the regions characterized by high ADCs at day 49 post QA injection, which were identified as necrotic regions in the histological study were relatively small. The failure of NAA levels to reach control levels even after 49 days may well be a manifestation of these small necrotic regions.

To conclude, in this study we found that the QA lesion exhibited ongoing pathological processes alongside regenerative processes for at least 70 days post QA injection. These processes were demonstrated by morphological, biochemical, behavioral and histological parameters. We therefore suggest that future studies using the QA rat model should take into consideration the spontaneous recovery of the different indices reported in this study.

Acknowledgements

The MRI scanner used in this study was purchased with grants from The Israel Science Foundation (ISF) and the Raymond and Beverly Sackler Institute of Biophysics of Tel Aviv University. We thank the Alfredo Federico Strauss Center for Computational NeuroImaging of Tel Aviv University. This work was funded in part by the Norma and Alan Aufzein Chair for Research in Parkinson's Disease.

REFERENCES

1. Stone TW. Endogenous neurotoxins from tryptophan. Toxicon 2001; 39: 61–73.
2. Schwarcz R, Whetsell WO, Mangano RM. Quinolinic acid - an endogenous metabolite that produces axon-sparing lesions in rat-brain. Science 1983; 219: 316–318.
3. Beal MF, Kowall NW, Ellison DW, Mazurek MF, Swartz KJ, Martin JB. Replication of the neurochemical characteristics of Huntington's disease by quinolinic acid. Nature 1986; 321: 168–171.
4. Alexi T, Borlongan CV, Faull RLM, Williams CE, Clark RG, Gluckman PD, Hughes PE. Neuroprotective strategies for basal ganglia degeneration: Parkinson's and Huntington's diseases. Prog. Neurobiol. 2000; 60: 409–470.
5. Mangiarini L, Sathasivam K, Seller M, Cozens B, Harper A, Hetherington C, Lawton M, Trottier Y, Lehrach H, Davies SW. and Bates GP. Exon 1 of the HD gene with an expanded CAG repeat is sufficient to cause a progressive neurological phenotype in transgenic mice. Cell 1996; 87: 493–506.
6. von Horsten S, Schmitt I, Nguyen HP, Holzmann C, Schmidt T, Walther T, Bader M, Pabst R, Kobbe P, Krotova J, Stiller D, Kask A, Vaarmann A, Rathke-Hartlieb S, Schulz JB, Grasshoff U, Bauer I, Vieira-Saecker AMM, Paul M, Jones L, Lindenberg KS, Landwehrmeyer B, Bauer A, Li XJ, Riess O. Transgenic rat model of Huntington's disease. Hum. Mol. Gen. 2003; 12: 617–624.
7. Dunnett SB, Rosser AE. Stem cell transplantation for Huntington's disease. Exp. Neurol. 2007; 203: 279–292.
8. Ramaswamy S, Shannon KM, Kordower JH. Huntington's disease: Pathological mechanisms and therapeutic strategies. Cell Transplant. 2007; 16: 301–312.
9. Wright BLC, Barker RA. Established and emerging therapies for Huntington's disease. Curr. Mol. Med. 2007; 7: 579–587.
10. Choi IY, Lee SP, Guilfoyle DN, Helpern JA. In vivo NMR studies of neurodegenerative diseases in transgenic and rodent models. Neurochem. Res. 2003; 28: 987–1001.
11. Moffett JR, Ross B, Arun P, Madhavarao CN, Namboodiri AMA. N-acetylaspartate in the CNS: From neurodiagnostics to neurobiology. Prog. Neurobiol. 2007; 81: 89–131.
12. Dautry W, Vaufrey F, Brouillet E, Bizat N, Henry PG, Conde F, Bloch G, Hantraye P. Early N-acetylaspartate depletion is a marker of neuronal dysfunction in rats and primates chronically treated with the mitochondrial toxin 3-nitropropionic acid. J. Cereb. Blood Flow Meta. 2000; 20: 789–799.
13. Demougeot C, Garnier P, Mossiat C, Bertrand N, Giroud M, Beley A, Marie C. N-Acetylaspartate, a marker of both cellular dysfunction and neuronal loss: its relevance to studies of acute brain injury. J. Neurochem. 2001; 77: 408–415.
14. Beal MF, Brouillet E, Jenkins BG, Ferrante RJ, Kowall NW, Miller JM, Storey E, Srivastava R, Rosen BR, Hyman BT. Neurochemical and histologic characterization of striatal excitotoxic lesions produced by the mitochondrial toxin 3-Nitropropionic acid. J. Neurosci. 1993; 13: 4181–4192.
15. Chyi T, Chang C. Temporal evolution of 3-nitropropionic acid-induced neurodegeneration in the rat brain by T-2-weighted, diffusion-weighted, and perfusion magnetic resonance imaging. Neurosci. 1999; 92: 1035–1041.
16. Lee WT, Lee CS, Pan YL, Chang C. Temporal changes of cerebral metabolites and striatal lesions in acute 3-nitropropionic acid intoxication in the rat. Magn. Reson. Med. 2000; 44: 29–34.
17. Lee WT, Shen YZ, Chang C. Neuroprotective effect of lamotrigine and MK-801 on rat brain lesions induced by 3-nitropropionic acid: Evaluation by magnetic resonance imaging and in vivo proton magnetic resonance spectroscopy. Neurosci. 2000; 95: 89–95.
18. Lee WT, Chang C. Magnetic resonance imaging and spectroscopy in assessing 3-nitropropionic acid-induced brain lesions: an animal model of Huntington's disease. Prog. Neurobiol. 2004; 72: 87–110.
19. Sauer D, Allegrini PR, Thedinga KH, Massieu L, Amacker H, Fagg GE. Evaluation of Quinolinic acid-induced excitotoxic neurodegeneration in rat striatum by quantitative magnetic-resonance-imaging in vivo. J. Neurosci. Methods 1992; 42: 69–74.
20. Guzman R, Meyer M, Lovblad KO, Ozdoba C, Schroth G, Seiler RW, Widmer HR. Striatal grafts in a rat model of Huntington's disease: Time course comparison of MRI and histology. Exp. Neurol. 1999; 156: 180–190.
21. Tkáč I, Keene CD, Pfeuffer J, Low WC, Gruetter R. Metabolic changes in quinolinic acid-lesioned rat striatum detected non-invasively by in vivo H-1 NMR spectroscopy. J. Neurosci. Res. 2001; 66: 891–898.
22. Strauss I, Williamson JM, Bertram EH, Lothman EW, Fernandez EJ. Histological and H-1 magnetic resonance spectroscopic imaging analysis of quinolinic acid-induced damage to the rat striatum. Magn. Reson. Med. 1997; 37: 24–33.
23. Sadan O, Shemesh N, Barzilay R, Bahat-Stromza M, Melamed E, Cohen Y, Offen D. Migration of neurotrophic factors-secreting mesenchymal stem cells towards a quinolinic acid lesion as viewed by MRI. Stem Cells 2008; 26: 2542–2551.
24. Paxinos G, Watson C. *The rat brain*, 4th ed. Academic Press: 1998.
25. Tkáč I, Starcuk Z, Choi IY, Gruetter R. In vivo H-1 NMR spectroscopy of rat brain at 1 ms echo time. Magn. Reson. Med. 1999; 41: 649–656.
26. Cobas JC, Sardina FJ. Nuclear magnetic resonance data processing. MestRe-C: A software package for desktop computers. Concepts Magn. Reson. Part A 2003; 19A: 80–96.
27. Carola V, D'Olimpio F, Brunamonti E, Mangia F, Renzi P. Evaluation of the elevated plus-maze and open-field tests for the assessment of anxiety-related behaviour in inbred mice. Behav. Brain Res. 2002; 134: 49–57.
28. de Almeida LP, Zala D, Aebischer P, Deglon N. Neuroprotective effect of a CNTF-expressing lentiviral vector in the quinolinic acid rat model of Huntington's disease. Neurobiol. Dis. 2001; 8: 433–446.

29. Alberch J, Perez-Navarro E, Canals JM. Neuroprotection by neurotrophins and GDNF family members in the excitotoxic model of Huntington's disease. Brain Res. Bull. 2002; 57: 817–822.
30. Dunnett SB. Functional analysis of fronto-striatal reconstruction by striatal grafts. Neural transplantation in neurodegenerative disease. Current Status and New Directions 2000; 231: 21–41.
31. Krenitsky TA, Dillberger J, Zotova E, Arezzo JC, Koprich JB, Mortazavi F, Gates TA, Dunbar GL. KP544, a nerve growth factor amplifier: Pharmacokinetics, safety, and efficacy in the rat. Drug Dev. Res. 2004; 62: 60–70.
32. Ryu JK, Choi HB, McLarnon JG. Combined minocycline plus pyruvate treatment enhances effects of each agent to inhibit inflammation, oxidative damage, and neuronal loss in an excitotoxic animal model of Huntington's disease. Neurosci. 2006; 141: 1835–1848.
33. Song J, Lee ST, Kang W, Park JE, Chu K, Lee SE, Hwang T, Chung H, Kim M. Human embryonic stem cell-derived neural precursor transplants attenuate apomorphine-induced rotational behavior in rats with unilateral quinolinic acid lesions. Neurosci. Lett. 2007; 423: 58–61.
34. Norris DG. The effects of microscopic tissue parameters on the diffusion weighted magnetic resonance imaging experiment. NMR Biomed. 2001; 1: 4.77–4.93.
35. Rudin M, Baumann D, Ekatodramis D, Stirnimann R, McAllister KH, Sauter A. MRI analysis of the changes in apparent water diffusion coefficient, T-2 relaxation time, and cerebral blood flow and volume in the temporal evolution of cerebral infarction following permanent middle cerebral artery occlusion in rats. Exp. Neurol. 2001; 169: 56–63.
36. Wick M, Nagatomo Y, Prielmeier F, Frahm J. Alteration of intracellular metabolite diffusion in rat-brain in-vivo during ischemia and reperfusion. Stroke 1995; 26: 1930–1933.
37. Duan WM, Widner H, Cameron RM, Brundin P. Quinolinic acid-induced inflammation in the striatum does not impair the survival of neural allografts in the rat. Euro. J. of Neurosci. 1998; 10: 2595–2606.
38. Guillemin GJ, Croitoru-Lamoury J, Dormont D, Armati PJ, Brew BJ. Quinolinic acid upregulates chemokine production and chemokine receptor expression in astrocytes. Glia 2003; 41: 371–381.
39. Hoehn M, Nicolay K, Franke C, van der Sanden B. Application of magnetic resonance to animal models of cerebral ischemia. J. Magn. Reson. Imaging 2001; 14: 491–509.
40. Sotak CH. Nuclear magnetic resonance (NMR) measurement of the apparent diffusion coefficient (ADC) of tissue water and its relationship to cell volume changes in pathological states. Neurochem. Int. 2004; 45: 569–582.
41. Moseley ME, Cohen Y, Mintorovitch J, Chileuitt L, Shimizu H, Kucharczyk J, Wendland MF, Weinstein PR. Early detection of regional cerebral-ischemia in cats–comparison of diffusion-weighted and T2-weighted MRI and spectroscopy. Magn. Reson. Med. 1990; 14: 330–346.
42. Ebisu T, Rooney WD, Graham SH, Weiner MW, Maudsley AA. N-Acetylaspartate as an in-vivo marker of neuronal viability in Kainate-induced status epilepticus - H-1 magnetic-resonance spectroscopic imaging. J. Cereb. Blood Flow Meta. 1994; 14: 373–382.
43. Higuchi T, Graham SH, Fernandez EJ, Rooney WD, Gaspary HL, Weiner MW, Maudsley AA. Effects of severe global ischemia on N-acetylaspartate and other metabolites in the rat brain. Magn. Reson. Med. 1997; 37: 851–857.
44. Kalra S, Cashman NR, Genge A, Arnold DL. Recovery of N-acetylaspartate in corticomotor neurons of patients with ALS after riluzole therapy. Neuroreport 1998; 9: 1757–1761.
45. Demougeot C, Bertrand N, Prigent-Tessier A, Garnier P, Mossiat C, Giroud M, Marie C, Beley A. Reversible loss of N-acetyl-aspartate in rats subjected to long-term focal cerebral ischemia. J. Cereb. Blood Flow Meta. 2003; 23: 482–489.
46. Tattersfield AS, Croon RJ, Liu YW, Kells AP, Faull RLM, Connor B. Neurogenesis in the striatum of the quinolinic acid lesion model of Huntington's disease. Neurosci. 2004; 127: 319–332.
47. Scattoni ML, Valanzano A, Popoli P, Pezzola A, Reggio R, Calamandrei G. Progressive behavioural changes in the spatial open-field in the quinolinic acid rat model of Huntington's disease. Behav. Brain Res. 2004; 152: 375–383.
48. Shear DA, Dong J, Gundy CD, Haik-Creguer KL, Dunbar GL. Comparison of intrastriatal injections of quinolinic acid and 3-nitropropionic acid for use in animal models of Huntington's disease. Prog Neuro-Psychopharmacology & Biological Psychiatry 1998; 22: 1217–1240.
49. Vinade ER, Schmidt AP, Frizzo MES, Portela LV, Soares FA, Schwalm FD, Elisabetsky E, Izquierdo I, Souza DO. Effects of chronic administered guanosine on behavioral parameters and brain glutamate uptake in rats. J. Neurosci. Res. 2005; 79: 248–253.